

Angular correlation function and scattering coefficient of electromagnetic waves scattered by a buried object under a two-dimensional rough surface

Guifu Zhang and Leung Tsang

Department of Electrical Engineering, Box 352500, University of Washington, Seattle, Washington 98195-2500

Kyung Pak

Jet Propulsion Laboratory, California Institute of Technology, 4800 Oak Grove Drive, Mail Stop 300-319, Pasadena, California 91109-8099

Received March 12, 1998; revised manuscript received August 3, 1998; accepted August 12, 1998

We study three-dimensional (3-D) electromagnetic wave scattering from a buried object under a two-dimensional (2-D) random rough surface. The surface integral equations of wave fields are used for the rough surface and the surface of the buried object. The surface fields are then solved by the method of moments. The scattered wave field from the object is represented by the rough-surface field so that the matrix equation can be solved efficiently by means of the sparse-matrix canonical-grid method. Numerical simulations are illustrated for a perfectly conducting sphere buried under a 2-D rough surface. Both the scattering coefficient (normalized radar cross section) and the angular correlation function (ACF) are calculated. The study of 3-D electromagnetic scattering allows the use of azimuthal angular averaging and the study of cross polarization and the polarization angular correlation function (PACF). It is found that the ACF is more effective in suppressing the clutter that is due to the rough-surface scattering, and the PACF is more useful for the detection of the buried object. © 1998 Optical Society of America [S0740-3232(98)00412-8]

OCIS codes: 290.0290, 290.5880.

1. INTRODUCTION

The study of electromagnetic wave scattering by a buried object under a random rough surface is of practical importance in both military and civil uses.¹⁻⁴ Wave scattering from random rough surfaces has been studied by means of analytical, experimental, and numerical methods.⁵⁻⁸ When an object is buried under a rough surface, both the rough surface and the object scatter waves in all directions, and mutual wave interaction between the rough surface and the object occurs. The contribution of the rough-surface scattering and the mutual interaction can be larger than or comparable to the scattering from the object. This makes the detection of the buried object difficult. It is important to know the wave scattering mechanism of the problem and to find an effective way to detect the buried object.

The wave scattering from a two-dimensional (2-D) object buried under a one-dimensional (1-D) rough surface has been numerically studied by using the method of moments^{9,10} (MoM). The wave scattering by a three-dimensional (3-D) object above and below a flat surface is studied by the *T*-matrix method.¹¹ Since most practical problems involve a 3-D object buried under a 2-D rough surface, a solution of electromagnetic wave scattering from a 2-D random rough surface with a 3-D buried object is needed. Recently the finite-difference time-domain method has been used in subsurface electromagnetic wave scattering problems.^{12,13} The solution of surface in-

tegral equations obtained with the MoM has been widely used in the study of rough-surface scattering problems. The difficulty in using the surface integral equation method with the MoM for 2-D rough-surface scattering problems is the large size of the impedance matrix, $6N \times 6N$, where N is the total number of points representing the surface. Furthermore, the solution time scales as $(6N)^3$ for the matrix inversion method.

To speed up the solution of surface integral equations with the MoM, fast methods have been used. The fast multipole and the fast Fourier transform have been combined for 2-D rough-surface scattering.¹⁴ Recently the sparse-matrix canonical-grid (SMCG) method has been developed for large-scale rough-surface scattering problems.¹⁵ The SMCG method has been used to study backscattering enhancement of electromagnetic wave scattering by 2-D perfectly conducting and dielectric rough surfaces.^{16,17}

Since the memory effect of wave scattering from random media was discovered by Feng *et al.* in 1988,¹⁸ the study of the angular correlation function (ACF) has attracted considerable attention.¹⁹⁻²¹ The ACF is the correlation function of two scattered fields in directions \hat{k}_{s2} and \hat{k}_{s1} corresponding to two incident waves in directions \hat{k}_{i2} and \hat{k}_{i1} , respectively. A strong correlation, called the angular memory effect, is exhibited only on the memory line for rough-surface scattering and on memory dots for volume scattering.¹⁹⁻²⁴ The values of the ACF away

from the memory line or dots are zero analytically and are very small experimentally and numerically. Therefore the ACF can be used for the detection of targets embedded in clutter if one avoids the memory effect.^{22–25}

Angular correlation functions are obtained by taking averages over a product of two signals. Thus a key step in calculating the ACF is taking averages. For random-media scattering, the average is usually taken over realizations of random media or rough surfaces, which is not applicable for detecting the object buried under a rough surface. For 2-D scattering problems of a target embedded in clutter, we have used frequency averaging and angular averaging to obtain the ACF.^{22–25} Numerical results have shown that detection of targets by the ACF with frequency and angular averaging has advantages over detection by the radar cross section (RCS).

Compared with previous work for 2-D scattering problems, the current study of the 3-D target detection problem is more difficult and more interesting. To formulate, wave fields satisfy vector equations in the 3-D case, whereas they are all scalar in the 2-D case. To solve the 3-D problem, a fast computation method has to be used because of the large number of unknowns, whereas matrix inversion was used in the 2-D cases. For averaging techniques, the 3-D problem has an additional degree of freedom resulting from a change of azimuthal angle. For a symmetric object, the wave statistics are also azimuthally symmetric. Hence azimuthal averaging has effects similar to realization averaging, giving wave statistics without changing the statistical characteristics. Since the scattering characteristics of the object and the rough surface are frequency dependent, the frequency averaging may blur the result. Therefore we use azimuthal angular averaging instead. The cross polarization and the polarization angular correlation function (PACF) can be studied in the 3-D cases; they were not encountered in the 2-D cases.

We study electromagnetic wave scattering by a 3-D buried object under a 2-D random rough surface. First we formulate the problem on the basis of the Stratton–Chu surface integral equations for the rough surface and the surface of the object. The coupled interaction between the rough surface and the object is included. Next the scattered wave fields from the object onto the rough surface are treated as additional incident fields on the rough surface. Then the SMCG method is used to solve the matrix equation. Numerical results are calculated for a perfectly conducting sphere under a rough surface. Both the ACF and the scattering coefficient are calculated for both co-polarization and cross polarization. To obtain the statistical results, we use azimuthal averaging. It is found that the ACF is more effective in suppressing the effects of the rough-surface scattering. The PACF is also studied; it is more useful for the detection of the buried object.

2. FORMULATION

A. Incident Wave

Consider an electromagnetic wave with fields $\mathbf{E}^i(x, y, z)$ and $\mathbf{H}^i(x, y, z)$, with time dependence $\exp(-i\omega t)$, impinging on a 2-D rough surface with a random-height pro-

file $z = f(xy)$. Above the rough surface is a free space (region 0), and the subsurface is characterized by permittivity ϵ_1 and permeability μ_1 (region 1). The height function $z = f(x, y)$ is a random process with zero mean. The incident direction is $\hat{k}_i = \sin \theta_i \cos \phi_i \hat{x} + \sin \theta_i \sin \phi_i \hat{y} - \cos \theta_i \hat{z}$. The incident wave is tapered so that the illuminated rough surface can be confined to the surface area $L_x \times L_y$. The incident electric and magnetic fields are given as

$$\begin{aligned} \mathbf{E}_\alpha^i(x, y, z) &= \int_{-\infty}^{+\infty} dk_x \int_{-\infty}^{+\infty} dk_y \\ &\times \exp(ik_x x + ik_y y - ik_z z) \\ &\times E_i(k_x, k_y) \hat{e}_\alpha(-k_z), \end{aligned} \quad (1)$$

and

$$\begin{aligned} \mathbf{H}_\alpha^i(x, y, z) &= -\frac{1}{\eta} \int_{-\infty}^{+\infty} dk_x \int_{-\infty}^{+\infty} dk_y \\ &\times \exp(ik_x x + ik_y y - ik_z z) \\ &\times E_i(k_x, k_y) \hat{h}_\alpha(-k_z) \end{aligned} \quad (2)$$

respectively, where α denotes horizontal polarization (h) and vertical polarization (v), given as

$$\begin{aligned} \hat{e}_h(-k_z) &= \frac{1}{k_\rho} (\hat{x} k_y - \hat{y} k_x), \\ \hat{h}_h(-k_z) &= \frac{k_z}{k k_\rho} (\hat{x} k_x + \hat{y} k_y) + \frac{k_\rho}{k} \hat{z}, \end{aligned} \quad (3)$$

$$\begin{aligned} \hat{e}_v(-k_z) &= \frac{k_z}{k k_\rho} (\hat{x} k_x + \hat{y} k_y) + \frac{k_\rho}{k} \hat{z}, \\ \hat{h}_v(-k_z) &= \frac{1}{k_\rho} (-\hat{x} k_y + \hat{y} k_x), \end{aligned} \quad (4)$$

where $k_z = (k^2 - k_x^2 - k_y^2)^{1/2}$ and $k_\rho = (k_x^2 + k_y^2)^{1/2}$ with k being the incident-wave number, η the intrinsic impedance of free space, and $E_i(k_x, k_y)$ the spectrum of the incident wave. We use the following spectrum,

$$\begin{aligned} E_i(k_x, k_y) &= \frac{1}{4\pi^2} \int_{-\infty}^{+\infty} dx \int_{-\infty}^{+\infty} dy \exp(-ik_x x - ik_y y) \\ &\times \exp[i(k_{ix} x + k_{iy} y)(1 + w)] \exp(-t), \end{aligned} \quad (5)$$

where $t = t_x + t_y = (x^2 + y^2)/g^2$ and

$$t_x = \frac{(\cos \theta_i \cos \phi_i x + \cos \theta_i \sin \phi_i y)^2}{g^2 \cos^2 \theta_i}, \quad (6)$$

$$t_y = \frac{(-\sin \phi_i x + \cos \phi_i y)^2}{g^2}, \quad (7)$$

$$w = \frac{1}{k^2} \left[\frac{(2t_x - 1)}{g^2 \cos^2 \theta_i} + \frac{(2t_y - 1)}{g^2} \right]. \quad (8)$$

The parameter g controls the tapering of the incident wave. The w and t terms are introduced to approximate the tapered-wave solution.

B. Surface Integral Equations

We apply Stratton–Chu surface integral equations on the rough surface and the surface of the buried object. For a rough surface with height function $z = f(x, y)$, we have the unit normal vector as

$$\hat{n} = \frac{1}{\left[\left(\frac{\partial f}{\partial x}\right)^2 + \left(\frac{\partial f}{\partial y}\right)^2 + 1\right]^{1/2}} \left(-\frac{\partial f}{\partial x} \hat{x} - \frac{\partial f}{\partial y} \hat{y} + 1 \hat{z}\right). \quad (9)$$

The boundary conditions for the dielectric rough surface are

$$\begin{aligned} \hat{n} \times \mathbf{E}_0 &= \hat{n} \times \mathbf{E}_1, & \hat{n} \times \mathbf{H}_0 &= \hat{n} \times \mathbf{H}_1 \\ \epsilon_0 \hat{n} \cdot \mathbf{E}_0 &= \epsilon_1 \hat{n} \cdot \mathbf{E}_1, & \mu_0 \hat{n} \cdot \mathbf{H}_0 &= \mu_1 \hat{n} \cdot \mathbf{H}_1 \end{aligned} \quad (10)$$

By noting that $\mu_0 = \mu_1$, we use Stratton–Chu equations approaching from both sides and the above boundary conditions. The integral equations on the rough surface are

$$\begin{aligned} \hat{n} \cdot \mathbf{E}^i(\mathbf{r}) &= \frac{\hat{n} \cdot \mathbf{E}(\mathbf{r})}{2} - \hat{n} \cdot \left\{ \int \hat{n}' \times \mathbf{H}(\mathbf{r}') i\omega\mu_0 g_0 dS' \right. \\ &\quad + P \int [(\hat{n}' \times \mathbf{E}(\mathbf{r}') \times \nabla g_0) \\ &\quad \left. + \nabla' g_0 \hat{n}' \cdot \mathbf{E}(\mathbf{r}')] dS' \right\}, \end{aligned} \quad (11)$$

$$\begin{aligned} \hat{n} \times \mathbf{H}^i(\mathbf{r}) &= \frac{\hat{n} \times \mathbf{H}(\mathbf{r})}{2} \\ &\quad - \hat{n} \times \left\{ \int -i\omega \hat{n}' \times \mathbf{E}(\mathbf{r}') \epsilon_0 g_0 dS' \right. \\ &\quad + P \int [\hat{n}' \times \mathbf{H}(\mathbf{r}') \\ &\quad \left. \times \nabla' g_0 + \hat{n}' \cdot \mathbf{H}(\mathbf{r}') \nabla' g_0] dS' \right\}, \end{aligned} \quad (12)$$

$$\begin{aligned} -\hat{n} \times \mathbf{E}_b^s(\mathbf{r}) &= -\frac{\hat{n} \times \mathbf{E}(\mathbf{r})}{2} \\ &\quad - \hat{n} \times \left(\int i\omega \hat{n}' \times \mathbf{H}(\mathbf{r}') \mu_1 g_1 dS' \right. \\ &\quad + P \int \left\{ [\hat{n}' \times \mathbf{E}(\mathbf{r}') \times \nabla' g_1] \right. \\ &\quad \left. + \left[\hat{n}' \cdot \mathbf{E}(\mathbf{r}') \frac{\epsilon_1}{\epsilon_0} \nabla' g_1 \right] \right\} dS' \Bigg), \end{aligned} \quad (13)$$

$$\begin{aligned} -\hat{n} \cdot \mathbf{H}_b^s(\mathbf{r}) &= -\frac{\hat{n} \cdot \mathbf{H}(\mathbf{r})}{2} \\ &\quad - \hat{n} \cdot \left(\int -\hat{n}' \times \mathbf{E}(\mathbf{r}') i\omega \epsilon_1 g_1 dS' \right. \\ &\quad + P \int \left\{ [\hat{n}' \times \mathbf{H}(\mathbf{r}') \times \nabla' g_1] \right. \\ &\quad \left. + \nabla' g_1 \hat{n}' \cdot \mathbf{H}(\mathbf{r}') \right\} dS' \Bigg), \end{aligned} \quad (14)$$

where the above integral $P \int$ represents the principal-value integral and g_0 and g_1 are the scalar Green's function in region 0 (air) and region 1 (lossy dielectric medium), respectively:

$$g_{0,1} = \frac{\exp(ik_{0,1}R)}{4\pi R}. \quad (15)$$

The distance between a field point \mathbf{r} and a source point \mathbf{r}' is

$$R = \{(x - x')^2 + (y - y')^2 + [f(x, y) - f(x', y')]^2\}^{1/2}.$$

In Eqs. (13) and (14), \mathbf{E}_b^s and \mathbf{H}_b^s are scattered fields from the buried object onto the rough surface. They are calculated as follows.

We assume that the buried object is a perfectly conducting sphere. It is convenient to use the magnetic field integral equation to solve the surface current on the object. For an exciting field of \mathbf{H}_b^e , the magnetic field integral equation for the surface current $\mathbf{J}_b = \hat{n}_b \times \mathbf{H}_b$ is

$$\hat{n}_b \times \mathbf{H}_b^e(\mathbf{r}) = \frac{\mathbf{J}_b(\mathbf{r})}{2} - \hat{n}_b \times \int_{S_b} \mathbf{J}_b(\mathbf{r}') \times \nabla' g_1 dS', \quad (16)$$

where the unit normal vector of the surface of the buried object is \hat{n}_b and the exciting field of \mathbf{H}_b^e for the buried object is the scattered field from the rough surface; i.e.,

$$\begin{aligned} \hat{n}_b \times \mathbf{H}_b^e(\mathbf{r}) &= -\hat{n}_b \times \int_{S_r} \{-\hat{n}' \times \mathbf{E}(\mathbf{r}') i\omega \epsilon_1 g_1 \\ &\quad + [\hat{n}' \times \mathbf{H}(\mathbf{r}') \times \nabla' g_1] \\ &\quad + \nabla' g_1 \hat{n}' \cdot \mathbf{H}(\mathbf{r}')\} dS'. \end{aligned} \quad (17)$$

Then the scattered fields from the buried object are expressed in terms of the surface current as

$$\mathbf{H}_b^s(\mathbf{r}) = \int_{S_b} \mathbf{J}_b(\mathbf{r}') \times \nabla' g_1 dS', \quad (18)$$

$$\mathbf{E}_b^s(\mathbf{r}) = \frac{-i}{\omega \epsilon_1} \nabla \times \int_{S_b} \mathbf{J}_b(\mathbf{r}') \times \nabla' g_1 dS'. \quad (19)$$

Equations (11)–(14) in combination with Eqs. (16)–(19) constitute the coupled integral equations between the rough surface and the buried object.

C. Matrix Equation and Its Solution

To solve the coupled integral equations, we discretize the rough surface and the surface of the object into small patches. For a patch at the rough surface, we use six knowns for the surface fields as follows:

$$\mathbf{J}_1(\mathbf{r}) = \mathbf{n} \times \mathbf{E}_r(\mathbf{r}) \cdot \hat{x}, \quad (20)$$

$$\mathbf{J}_2(\mathbf{r}) = \mathbf{n} \times \mathbf{E}_r(\mathbf{r}) \cdot \hat{y}, \quad (21)$$

$$\mathbf{J}_3(\mathbf{r}) = \mathbf{n} \cdot \mathbf{E}_r(\mathbf{r}), \quad (22)$$

$$\mathbf{J}_4(\mathbf{r}) = \mathbf{n} \times \mathbf{H}_r(\mathbf{r}) \cdot \hat{x}, \quad (23)$$

$$\mathbf{J}_5(\mathbf{r}) = \mathbf{n} \times \mathbf{H}_r(\mathbf{r}) \cdot \hat{y}, \quad (24)$$

$$\mathbf{J}_6(\mathbf{r}) = \mathbf{n} \cdot \mathbf{H}_r(\mathbf{r}). \quad (25)$$

If we use the above definitions for unknowns and the MoM, Eqs. (11)–(14) become a matrix equation:

$$\bar{\bar{Z}}\bar{J} = \bar{b}_i + \bar{b}_b, \quad (26)$$

where the impedance matrix of the rough surface is $\bar{\bar{Z}}$, \bar{b}_i represents incident fields, and \bar{b}_b represents scattered fields from the buried object. We discretize the surface of the object and use the following definition for the surface current on the object.

Let $\bar{\bar{Z}}_b$ be the impedance matrix for the buried object, $\bar{\bar{Z}}_{rb}$ be the impedance matrix from the buried object to the rough surface, and $\bar{\bar{Z}}_{br}$ be the impedance matrix from the rough surface to the buried object. Then it follows from Eqs. (16)–(19) that

$$J_{b1}(\mathbf{r}) = \hat{n}_b \times \mathbf{H}_b(\mathbf{r}) \cdot \hat{x}, \quad (27)$$

$$J_{b2}(\mathbf{r}) = \hat{n}_b \times \mathbf{H}_b(\mathbf{r}) \cdot \hat{y}, \quad (28)$$

$$J_{b3}(\mathbf{r}) = \hat{n}_b \times \mathbf{H}_b(\mathbf{r}) \cdot \hat{z}, \quad (29)$$

and from Eqs. (17)–(20) we have

$$\bar{b}_b = \bar{\bar{Z}}_{rb}\bar{J}_b = \bar{\bar{Z}}_{rb}\bar{\bar{Z}}_b^{-1}\bar{J}_b^e = \bar{\bar{Z}}_{rb}\bar{\bar{Z}}_b^{-1}\bar{\bar{Z}}_{br}\bar{J}. \quad (30)$$

Substituting Eq. (30) into (26), we get

$$(\bar{\bar{Z}} - \bar{\bar{Z}}_{rb}\bar{\bar{Z}}_b^{-1}\bar{\bar{Z}}_{br})\bar{J} = \bar{b}_i. \quad (31)$$

In principle, Eq. (31) is then ready for solution by matrix inversion. The problem is that the matrix inversion for a large number of unknowns becomes computationally formidable. Thus the following efficient sparse-matrix canonical-grid (SMCG) method is used.

To speed up the solution of Eq. (31), we decompose the impedance matrix for the rough surface $\bar{\bar{Z}}$ into three parts: a block Toeplitz flat-surface part $\bar{\bar{Z}}^{FS}$, a strong-interaction part $\bar{\bar{Z}}^S$, and the weak remainder $\bar{\bar{Z}}^W$. With the weak-remainder part moved to the right-hand side, we have

$$(\bar{\bar{Z}}^{FS} + \bar{\bar{Z}}^S - \bar{\bar{Z}}_{rb}\bar{\bar{Z}}_b^{-1}\bar{\bar{Z}}_{br})\bar{J} = \bar{b}_i - \bar{\bar{Z}}^W\bar{J}. \quad (32)$$

Equation (32) is then solved by the conjugate-gradient method with an updated right-hand side.

For a small object, the solution of Eq. (32) can be further speeded up with the buried-object term moved to the right-hand side, as given by

$$(\bar{\bar{Z}}^{FS} + \bar{\bar{Z}}^S)\bar{J} = \bar{b}_i + \bar{\bar{Z}}_{rb}\bar{\bar{Z}}_b^{-1}\bar{\bar{Z}}_{br}\bar{J} - \bar{\bar{Z}}^W\bar{J}. \quad (33)$$

The new matrix equations (32) and (33) are solved with the conjugate-gradient method.²¹ The product of $\bar{\bar{Z}}^{(FS)}$ with \bar{J} can be computed with a 2-D fast-Fourier-transform algorithm, which makes conjugate-gradient iteration efficient. An update of the right-hand side is also quickly calculated. The iteration is terminated when the error-norm criterion is less than 0.2%.

D. Statistics of Scattered Fields

After the surface currents are solved, the scattered fields in medium 0 can be calculated. The scattering amplitudes for both co-polarization and cross polarizations $F_{\beta\alpha}$ are, respectively,

$$F_{h\alpha} = \frac{ik}{4\pi\sqrt{2}\eta P_\alpha^i} \int_{dS'} dx' dy' \times \exp(-ik\gamma') \left\{ \left[J_1(x', y') \cos \theta_s \cos \phi_s + J_2(x', y') \cos \theta_s \sin \theta_s - J_1(x', y') \frac{\partial f(x', y')}{\partial x'} \sin \theta_s - J_2(x', y') \frac{\partial f(x', y')}{\partial y'} \sin \theta_s \right] - \eta [J_4(x', y') \sin \phi_s - J_5(x', y') \cos \phi_s] \right\} \quad (34)$$

and

$$F_{v\alpha} = \frac{ik}{4\pi\sqrt{2}\eta P_\alpha^i} \int_{dS'} dx' dy' \times \exp(-ik\gamma') \left\{ [J_1(x', y') \sin \phi_s - J_2(x', y') \cos \phi_s] + \eta \left[J_4(x', y') \cos \theta_s \cos \theta_s + J_5 \cos \theta_s \sin \phi_s - J_4(x', y') \frac{\partial f(x', y')}{\partial x'} \sin \theta_s - J_5(x', y') \frac{\partial f(x', y')}{\partial y'} \sin \theta_s \right] \right\}, \quad (35)$$

where $\gamma' = x' \sin \theta_s \cos \phi_s + y' \sin \theta_s \sin \phi_s + f(x', y') \cos \theta_s$. Note that the scattering amplitudes are normalized by the square root of the incident power $2\eta P_{i\alpha}$ as

$$P_\alpha^i = \frac{2\pi^2}{\eta} \int_{k_\rho < k} dk_x dk_y |E_{i\alpha}(k_x, k_y)|^2 \frac{k_z}{k}. \quad (36)$$

Since the buried object is under a single random rough surface, realization averaging is not applicable. Both the bistatic scattering coefficient (normalized RCS) and the ACF are calculated on the basis of azimuthal averaging as follows:

$$\sigma_{\beta\alpha}(\theta_s, \theta_i) = \frac{1}{N_\phi} \sum_{n=1}^{N_\phi} |F_{\beta\alpha}(\theta_s, \phi_{sn}; \theta_i, \phi_{in})|^2, \quad (37)$$

$$\Gamma_{\beta\alpha}(\theta_{s2}, \theta_{i2}; \theta_{s1}, \theta_{i1})$$

$$= \frac{1}{N_\phi} \sum_{n=1}^{N_\phi} F_{\beta\alpha}(\theta_{s2}, \phi_{s2n}; \theta_{i2}, \phi_{i2n}) \times F_{\beta\alpha}^*(\theta_{s1}, \phi_{s1n}; \theta_{i1}, \phi_{i1n}), \quad (38)$$

where ϕ_{in} and ϕ_{sn} are incident and scattering azimuthal angles, respectively. In the scattering plane, they are related to each other as follows: (i) $\phi_{sn} = \phi_{in}$ for θ_s and θ_i having the same sign and (ii) $\phi_{sn} = \phi_{in} + 180^\circ$ for θ_s and θ_i having opposite signs.

For the case of θ_s and θ_i with the same sign, the bistatic scattering is in the forward direction. For this case we make ϕ_s and ϕ_i the same. The averaging is performed over different ϕ . This means that the source and observation directions are to be rotated in a circular geometry over the target. For the case of θ_s and θ_i having opposite signs, this is the backward direction, and we make ϕ_s and ϕ_i differ by 180° : source and observation are in the same backward direction and are rotated for different ϕ .

Equation (38) can be extended to calculate the PACF as follows:

$$\begin{aligned} & \Gamma_{\beta_1\alpha_1\beta_2\alpha_2}(\theta_{s1}, \theta_{i1}; \theta_{s2}, \theta_{i2}) \\ &= \frac{1}{N_\phi} \sum_{n=1}^{N_\phi} F_{\beta_1\alpha_1}(\theta_{s1}, \phi_{s1n}; \theta_{i1}, \phi_{i1n}) \\ & \quad \times F_{\beta_2\alpha_2}^*(\theta_{s2}, \phi_{s2n}; \theta_{i2}, \phi_{i2n}). \quad (39) \end{aligned}$$

3. RESULTS AND DISCUSSION

The numerical simulation is conducted for a perfectly electrical conducting (PEC) sphere buried under a 2-D Gaussian random rough surface (see Fig. 1). The rough surface is generated by using the spectrum method with the assumption of a Gaussian spectrum. The sizes of the rough surface in the x and y directions are $L_x = L_y = 8.0\lambda$, respectively. The surface rms heights are $h_x = h_y = 0.02\lambda$, and the correlation lengths are $l_x = l_y = 0.5\lambda$. The tapering parameter is $g = L_x/4 = L_y/4$. The relative dielectric constant of the lower medium is $\epsilon_r = (2.0 + i0.2)$. The surface is sampled at 64 points per λ^2 to give 24,576 surface unknowns. The neighborhood distance $r_d = 3.5\lambda$. A sphere of radius $a = 0.3\lambda$ is buried under the rough surface at a depth $d = 0.6\lambda$. The sphere surface is discretized into 80 triangle patches as shown in Fig. 2, for which the surface currents are represented by 240 unknowns. The impedance matrix of the sphere \bar{Z}_b is calculated and tested by calculating the scattering cross section of a sphere in free space. The numerical results agree with those obtained by Mie scattering, as shown in Fig. 3.

We solve the matrix equations with the buried-object contribution on the left-hand side [Eq. (32)] and on the right-side [Eq. (33)]; the two equations give the same result. The scattering coefficients are shown in Fig. 4. The CPU with the target term on the right-hand side is five times faster than the CPU with the target term on the left-hand side.

We calculate the scattering amplitudes for ten azimuthal angles at $0^\circ, 36^\circ, \dots, \text{and } 324^\circ$. The RCS and the ACF are calculated by using azimuthal angular averaging as given in Eqs. (37) and (38). We plot the results as functions of the scattering angle θ_{s2} . Parameters for other angles are $\theta_{i1} = 20^\circ$, $\theta_{s1} = -40^\circ$, and $\theta_{i2} = 20^\circ$. Figure 5 shows the results for the hh polarization (co-

polarization) component. The results both with and without the target sphere are shown for comparison. Figure 5(a) is for the RCS, and, as expected, there is a peak in the specular direction, which is due to the slightly rough surface. The difference between the RCS with and without the target is large only for large scattering angles, since the rough-surface scattering is small in

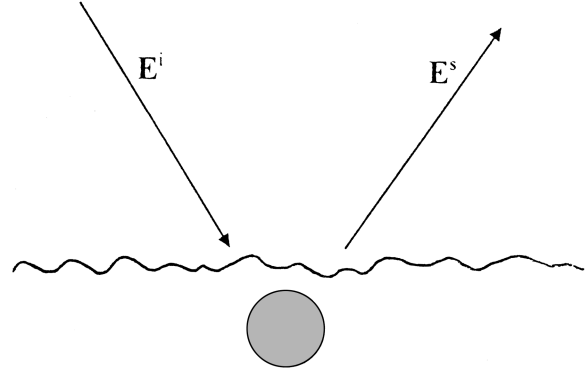


Fig. 1. Configuration of EM wave scattering by a 3-D object buried under a 2-D rough surface.

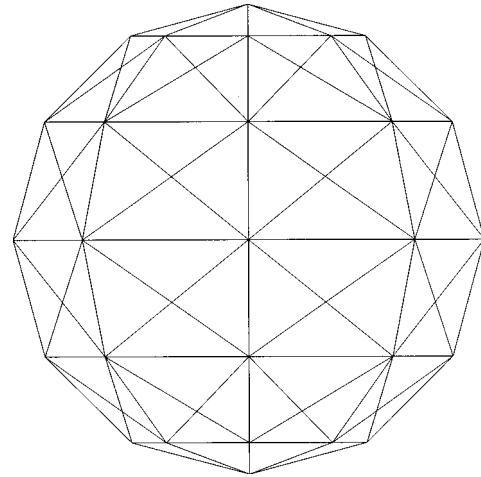


Fig. 2. Discretization of a sphere into 80 triangle patches.

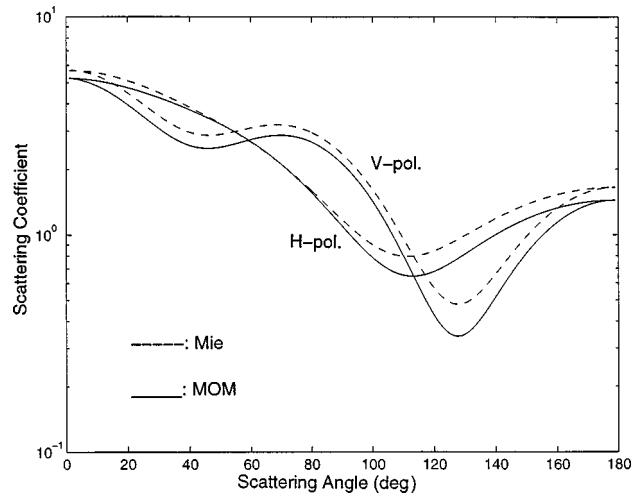


Fig. 3. Comparison of MoM and Mie scattering for the RCS of a PEC sphere ($a = 0.36$).

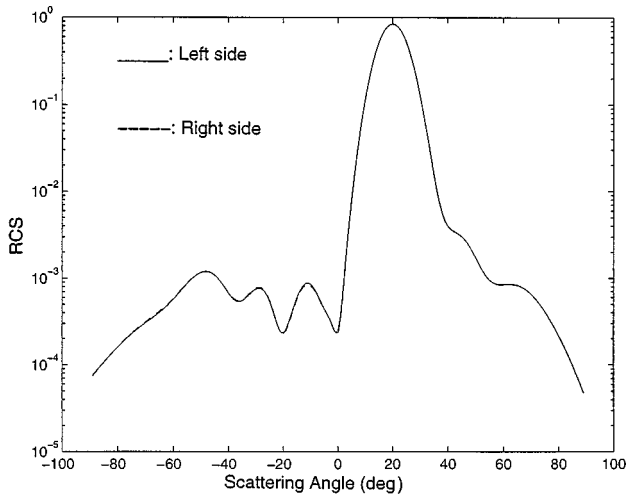


Fig. 4. Comparison of the solution of the matrix equation for the object on the left-hand side and the object on the right-hand side.

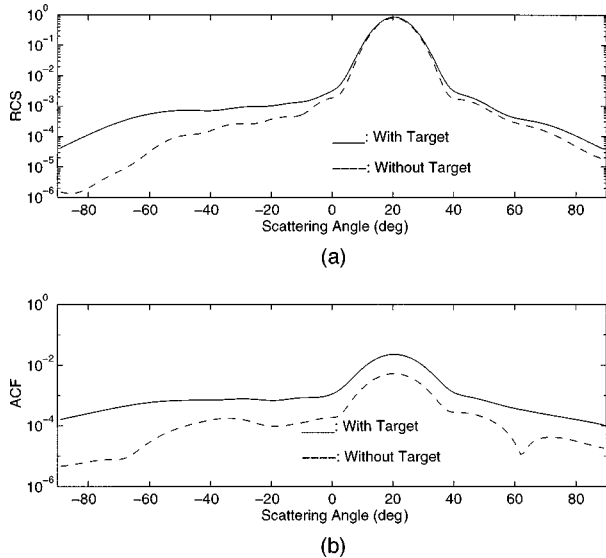


Fig. 5. (a) RCS and (b) ACF for EM wave scattering by a PEC sphere buried under a 2-D rough surface for the *hh* polarization component. Parameters are $a = 0.3\lambda$, $d = 0.6\lambda$, $L_x = L_y = 8.0\lambda$, $h = 0.02\lambda$, $l_x = l_y = 0.5.0\lambda$, $r_d = 3.5\lambda$, $g = L_x/4 = L_y/4$, $\theta_{i1} = 20^\circ$, $\theta_{s1} = -40^\circ$, and $\theta_{i2} = 20^\circ$.

these cases. As shown in Fig. 5(b), however, the difference for the ACF can be as high as 7 dB even for angles closed to the nadir direction. This is because the memory effect is avoided and rough surface scattering is minimized.

The fully polarimetric results for RCS and the ACF were calculated and are shown in Figs. 6 and 7, respectively. In Fig. 6 we see that the differences between the RCS with and without a target for co-polarizations are larger than those for cross polarizations. This is because the cross-polarization components are due mainly to the rough-surface scattering. Because the target is a sphere, it has only a small cross-polarization contribution. It can also be found that there are larger differences for the *vv* component than for the *hh* component, since the vertical polarization wave has better penetration through the surface. In Fig. 7 we can see the big difference between the

ACF with and without a target in both the co-polarization and cross-polarization results. This is because of the random phase of rough-surface scattering that is included in the ACF calculation. The results for the polarization angular correlation function (PACF) were also calculated and are shown in Fig. 8. Figure 8(a) shows the PACF for *hh* and *vh* components. Figure 8(b) shows the PACF for *vv* and *hv* components. We can see an even larger difference from the ACF up to 10–20 dB.

Whether an object is hidden by a rough surface depends on factors such as beam size, dielectric constant,

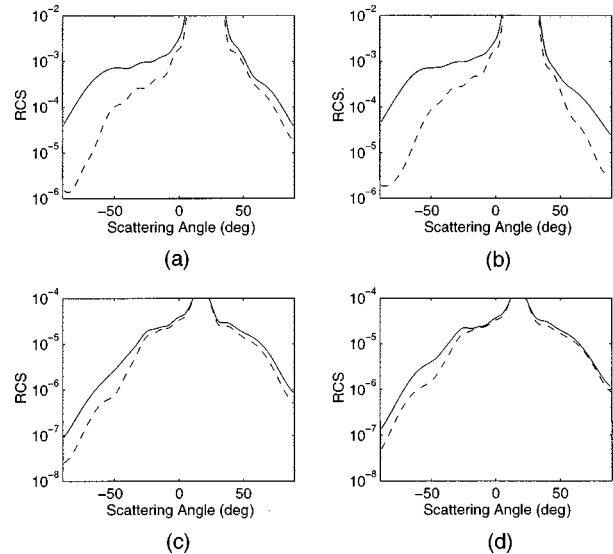


Fig. 6. RCS for EM wave scattering by a PEC sphere buried under a 2-D rough surface for co-polarized and cross-polarized components. (a) *hh*, (b) *vv*, (c) *vh*, (d) *hv*. Parameters are $a = 0.3\lambda$, $d = 0.6\lambda$, $L_x = L_y = 8.0\lambda$, $h = 0.02\lambda$, $l_x = l_y = 0.5.0\lambda$, $r_d = 3.5\lambda$, $g = L_x/4 = L_y/4$, $\theta_{i1} = 20^\circ$, $\theta_{s1} = -40^\circ$, and $\theta_{i2} = 20^\circ$.

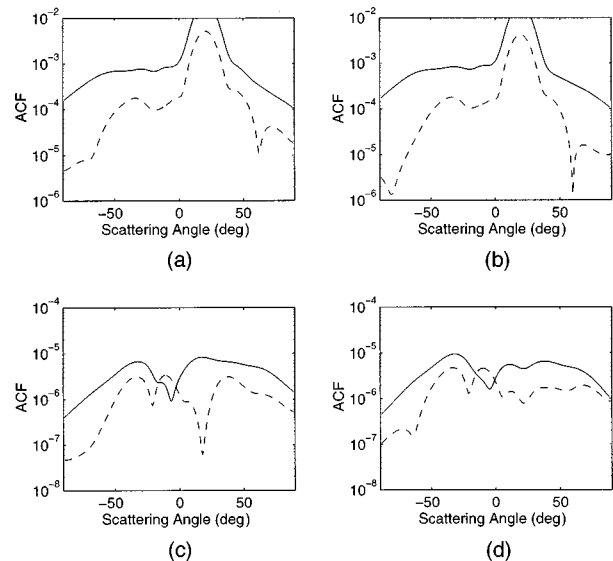


Fig. 7. ACF for EM wave scattering by a PEC sphere buried under a 2-D rough surface for co-polarized and cross-polarized components. (a) *hh*, (b) *vv*, (c) *vh*, (d) *hv*. Parameters are $a = 0.3\lambda$, $d = 0.6\lambda$, $L_x = L_y = 8.0\lambda$, $h = 0.02\lambda$, $l_x = l_y = 0.5.0\lambda$, $r_d = 3.5\lambda$, $g = L_x/4 = L_y/4$, $\theta_{i1} = 20^\circ$, $\theta_{s1} = -40^\circ$, and $\theta_{i2} = 20^\circ$.

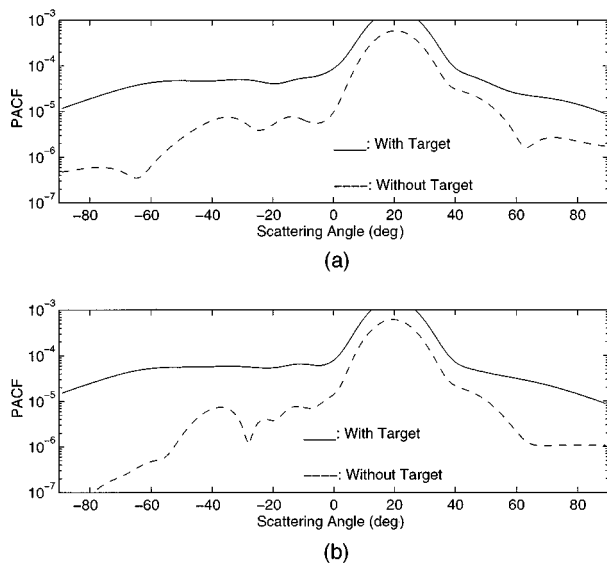


Fig. 8. PACF for EM wave scattering by a PEC sphere buried under a 2-D rough surface with co-polarized and cross-polarized components. (a) $hhvh$, (b) $vvhu$. Parameters are $a = 0.3\lambda$, $d = 0.6\lambda$, $L_x = L_y = 8.0\lambda$, $h = 0.02\lambda$, $l_x = l_y = 0.5.0\lambda$, $r_d = 3.5\lambda$, $g = L_x/4 = L_y/4$, $\theta_{i1} = 20^\circ$, $\theta_{s1} = -40^\circ$, and $\theta_{i2} = 20^\circ$.

object size, buried depth, and rms height and slope. For a slightly random rough surface, the wave scattering by the object around the specular direction and in the vicinity of the specular direction is obscured by the surface. This is shown in Figs. 5 and 6. The dependence on the width of incident beam is a result of rough-surface scattering, which is proportional to the illumination area for large surfaces. Therefore the wider the incident beam, the larger the rough surface being illuminated and the more difficult it is to detect the object. The same explanation can be given for the effect of the distance between the detector and the rough surface. The dependences on dielectric constant, object size, and buried depth have been studied for 2-D cases.²⁴ Numerical verification for the 3-D case requires more computer resources, because a wider incident beam corresponds to a larger rough surface and there are more unknowns to be solved from Maxwell's equation.

In this paper we studied electromagnetic wave scattering from a 3-D buried object under a 2-D random rough surface, using the formulation of surface integral equations. The surface fields were solved by the MoM. The scattered-wave field from the object was represented by the rough surface field so that the matrix equation could be solved efficiently by using the sparse-matrix canonical-grid method. Numerical simulations were given for a PEC sphere buried under a 2-D rough surface. Both the RCS and the ACF were calculated on the basis of azimuthal angular averaging. Results show that the ACF is more effective than the RCS in suppressing the clutter that is due to rough-surface scattering and that the cross-polarization components of the ACF can also be used for target detection. The PACF can be even more effective than the ACF for target detection.

ACKNOWLEDGMENT

This research was supported by the U.S. Office of Naval Research under contract N00014-97-1-0813.

Guifu Zhang is currently with the National Center for Atmospheric Research, P.O. Box 3000, Boulder, Colorado 80307-3000. Telephone, 303-497-8397; fax, 303-497-8401; e-mail, guzhang@rap.ucar.edu. L. Tsang can be reached at the address on the title page and by telephone, 206-685-7537; fax, 206-543-3842; and e-mail, tsang@ee.washington.edu.

REFERENCES

1. L. Peters, J. Daniels, and J. Young, "Ground penetrating radar as a subsurface environmental sensing tool," *Proc. IEEE* **82**, 1802–1822 (1994).
2. S. Vitebskiy, L. Carin, M. A. Ressler, and F. H. Le, "Ultra-wideband, short-pulse ground-penetrating radar: simulation and measurement," *IEEE Trans. Geosci. Remote Sens.* **35**, 762–772 (1997).
3. X. Yang, D. A. Gregory, and P. S. Erbach, "Clutter reduction and target detection enhancement using wavelet transform techniques," in *Optical Pattern Recognition VI*, D. P. Casasent and T.-H. Chao, eds., *Proc. SPIE* **2490**, 125–139 (1995).
4. Y. Yamaguchi and T. Moriyama, "Polarimetric detection of objects buried in snowpack by a synthetic aperture FM-CM radar," *IEEE Trans. Geosci. Remote Sens.* **34**, 45–51 (1996).
5. A. Ishimaru, *Wave Propagation and Scattering in Random Media* (Academic, New York, 1978), Vols. I and II.
6. L. Tsang, J. A. Kong, and R. T. Shin, *Theory of Microwave Remote Sensing* (Wiley-Interscience, New York, 1985).
7. L. Tsang, C. H. Chan, and K. Pak, "Backscattering enhancement of a two-dimensional random rough surface (three-dimensional scattering) based on Monte Carlo simulations," *J. Opt. Soc. Am. A* **11**, 711–715 (1994).
8. P. Tran and A. A. Maradudin, "The scattering of electromagnetic waves from 2D metallic surface," *Opt. Commun.* **110**, 269–273 (1994).
9. K. O'Neill, R. Lussky, and K. D. Paulsen, "Scattering from a metallic reflector embedded in a lossy dielectric beneath a random rough surface," *IEEE Trans. Geosci. Remote Sens.* **34**, 367–376 (1996).
10. A. Madrazo and M. Nieto-Vesperinas, "Scattering of light and other electromagnetic waves from a body buried beneath a highly rough random surface," *J. Opt. Soc. Am. A* **14**, 1859–1866 (1997).
11. G. Videen, "Light scattering from a sphere behind a plane," *J. Opt. Soc. Am. A* **10**, 110–117 (1993).
12. S. Tjuatja, A. K. Fung, S. Wu, P. Zhou, and Z. Li, "Remote sensing of buried objects: an analysis using FD-TD simulation," presented at the International Geoscience and Remote Sensing Symposium '97, Singapore, August 3–8, 1997.
13. Y. H. Chen, W. C. Chew, and M. L. Oristaglio, "Application of perfectly matched layers to the transient modeling of subsurface EM problems," *Geophysics* **62**, 1730–1736 (1997).
14. R. L. Wagner, J. Song, and W. C. Chew, "Monte Carlo simulation of electromagnetic scattering from two-dimensional random rough surfaces," *IEEE Trans. Antennas Propag.* **45**, 235–245 (1997).
15. K. Pak, "Studies of large-scale random rough surface scattering problems based on Monte Carlo simulations with efficient computational integral equation methods," Ph.D. dissertation (University of Washington, Seattle, Wash., 1996).
16. K. Pak, L. Tsang, C. H. Chan, and J. Johnson, "Backscattering enhancement of electromagnetic waves from two-dimensional perfectly conducting random rough sur-

- faces based on Monte Carlo simulations," *J. Opt. Soc. Am. A* **12**, 2491–2499 (1995).
17. K. Pak, L. Tsang, and J. Johnson, "Numerical simulations and backscattering enhancement of scattered waves from two-dimensional dielectric random rough surfaces with sparse-matrix canonical grid method," *J. Opt. Soc. Am. A* **14**, 1515–1529 (1997).
 18. S. Feng, C. Kane, P. A. Lee, and A. D. Stone, "Correlations and fluctuations of coherent wave transmission through disordered media," *Phys. Rev. Lett.* **61**, 834–837 (1988).
 19. T. R. Michel and K. A. O'Donnell, "Angular correlation functions of amplitudes scattered from a one-dimensional, perfectly conducting rough surface," *J. Opt. Soc. Am. A* **9**, 1374–1384 (1992).
 20. M. Nieto-Vesperinas and J. A. Sanchez-Gil, "Intensity angular correlations of light multiply scattered from random rough surfaces," *J. Opt. Soc. Am. A* **10**, 150–157 (1993).
 21. A. A. Maradudin, M. Nieto-Vesperinas, and E. Thorsos, "Enhanced backscattering of light from randomly rough surfaces and related phenomena I: one-dimensional surfaces and angular correlation function of scattered fields," *Comments Condens. Matter Phys.* **17**, 13–37 (1994).
 22. L. Tsang, G. Zhang, and K. Pak, "Detection of a buried object under a single random rough surface with angular correlation function in EM wave scattering," *Microwave Opt. Technol. Lett.* **11**, 300–304 (1996).
 23. G. Zhang, L. Tsang, and Y. Kuga, "Angular correlation function of wave scattering by a buried object embedded in random discrete scatterers under a rough surface," *Microwave Opt. Technol. Lett.* **14**, 144–151 (1997).
 24. G. Zhang, L. Tsang, and Y. Kuga, "Studies of the angular correlation function of scattering by random rough surfaces with and without a buried object," *IEEE Trans. Geosci. Remote Sens.* **35**, 444–453 (1997).
 25. G. Zhang and L. Tsang, "Application of the angular correlation function of clutter scattering and correlation imaging in target detection," *IEEE Trans. Geosci. Remote Sens.* **36**(5) (1998).